Crystal electric field and magnetic-ion–lattice interactions in TmZn

P. Morin
Laboratoire de Magnétisme, C.N.R.S., 166 X, 38042-Grenoble-Cedex, France

A. Waintal
Laboratoire des Rayons X et Service National des Champs Intenses, C.N.R.S., 166 X, 38042-Grenoble-Cedex, France

B. Lüthi*
Physics Department, Rutgers University, New Brunswick, New Jersey 08903
(Received 2 February 1976)

Experimental results on magnetic and elastic properties for the cubic intermetallic compound TmZn are presented. The magnetic-susceptibility measurement gives a ferromagnetic ordering temperature of $T_c = 10$ K and an effective Bohr magneton number $g[J(J+1)]^{1/2} = 7.67$. We can interpret the high-field (up to 125 kOe) magnetization curves for $T < T_c$ using the crystal-field split $^3H_6$ ground state for the Tm^{3+} ion. For the cubic crystal-field parameters we obtain $A_4\langle r^4\rangle = -170 \pm 20$ K, $A_6\langle r^6\rangle = -10 \pm 3$ K. The elastic constant $c_{11} - c_{12}$ shows a softening of 40% from room temperature down to 13 K. The c_{44} mode and the bulk modulus show a normal temperature dependence for $T > T_c$. We interpret the temperature dependence of the $c_{11} - c_{12}$ mode as due to a crystal-field effect, which is particularly pronounced in TmZn because the crystal-field ground state is a doublet Γ_3. The magnetoelastic coupling constant $g_2^2 = 8.9$ mK together with an additional quadrupole-quadrupole coupling constant $g' = -9.6$ mK are not strong enough to induce a structural transition in the absence of exchange interactions. We compare these results to the recently investigated TmCd compound, which exhibits no magnetic transition but a structural transition at $T_a = 3.16$ K.

I. INTRODUCTION

The equiatomic compounds of the rare earths with divalent metals like zinc (RZn) have the cubic CsCl structure. This simple structure enables one to study the different interactions of the $4f$ shell in a metallic surrounding. Recently, various measurements on single crystals of these compounds have been performed: magnetic,[1] dilatometric,[2] specific-heat,[3] and inelastic-neutron-scattering[4] experiments. In all these experiments the effect of the crystalline electric field (CEF) was shown to be important. With the various experimental techniques the level scheme could be determined for the RZn intermetallics. It was found that the CEF parameters A_4 and A_6 are negative for the RZn. However, their variation across the series is complicated and does not follow simple point-charge model predictions. This is somewhat analogous to the case of rare earths in[5,6] Ag and in Au or in Y and Sc,[7] but differs from the situation in the rare-earth pnictides.[8]

The light RZn compounds (R-Ce, Pr, Nd) order antiferromagnetically, whereas the heavier RZn order ferromagnetically with ordering temperatures T_c ranging from 10 (TmZn) to 271 K (GdZn).[9] The strong exchange interaction is presumably of the indirect type, the large density of $5d$ electrons may induce the main coupling to the $4f$ shell[10] and contribute both to the CEF parameters[9] and to an anisotropic exchange term. In addition to this strong exchange effect, lattice distortions were observed in some cases below the ordering temperature,[2] indicating strong quadrupole-strain effects.

It is the purpose of this paper to present a detailed study of magnetic and elastic properties of TmZn. In particular we would like to give experimental results for the magnetic susceptibility, the magnetization in high fields along different crystallographic directions and for the temperature dependence of the elastic constants. From these experiments we are able to deduce the CEF level scheme and various magnetoelastic and quadrupole-quadrupole coupling constants. The main result of this study is a quantitative explanation of the magnetic properties and of the temperature dependence of the elastic constants, proving a quadrupole-quadrupole interaction. A list of physical constants deduced from these experiments is shown in Table I.

TmZn is an interesting substance for such a study, because it has a low $T_c = 10$ K, enabling us to study CEF effects both in the ordered and in the paramagnetic states. Furthermore the related compound TmCd has been studied recently in a similar way.[11] It is therefore interesting to compare the two substances.

In Sec. II we describe the experimental methods. Afterwards we present and analyze the magnetic and lattice properties. Finally, we discuss these results.

II. EXPERIMENTAL METHODS

TmZn was obtained by direct fusion of the two components in a sealed tantalum crucible and by cooling from the melt in a Bridgman furnace; the temperature gradient was about 20 °C/cm. By this method we obtained single crystals of good size. Spheres of about 3 mm in diameter were spark cut and used for magnetic measurements. For the ultrasonic experiments we cut a cylindrical sample oriented along a twofold axis and polished the two parallel cross sections. The diameter of the sample was about 5 mm and the length 6 mm.

We have studied the magnetization in the ordered state along the three principal axes of the cubic cell in fields up to 150 kOe, using the facilities of the Service National des Champs Intenses at Grenoble. The field was produced by a 5-MW Bitter coil and the magnetization was measured by a conventional flux method. The susceptibility measurements were performed at the Laboratoire de Magnétisme with a translation balance in a thermal range from helium temperature up to 650 K.

The elastic constants were determined from velocity measurements of ultrasonic longitudinal and transverse waves propagated along the $\langle 110\rangle$ direction of the sample. The pulse-echo overlap method was used.[12] The transducers were X-cut and Y-cut quartz disks with a fundamental frequency of either 10, 15, or 20 MHz. The transducers were bound to the sample with Nonaq stopcock grease. Temperatures were measured with a platinum thermometer in the range 40–300 K and with a carbon one below 40 K. Data were taken from 300 K down to the transition temperature of 10 K and in some cases below T_c. In particular, in order to measure the $c_{11}-c_{12}$ elastic constant, we had to reduce the sample thickness because of the strong attenuation at low temperatures close to T_c. No thermal-expansion corrections were necessary, the fractional velocity changes being always much larger than the fractional length changes.

III. RESULTS AND DISCUSSION

A. Magnetic properties: Experiment

The determination of the ordering temperature was obtained in a constant field of 100 Oe: below a Curie temperature of $T_c = 10$ K, we observed ferromagnetic behavior (inset, Fig. 1). Above, the reciprocal susceptibility follows a Curie-Weiss law up to 650 K with a paramagnetic moment of $7.67\mu_B$ close to the free-ion value $g[J(J+1)]^{1/2} = 7.57\mu_B$ (Fig. 1). The slight difference between these two values may correspond partly to the band Pauli susceptibility. Note that the paramagnetic Curie temperature is $\Theta_p = 0$ K; in all the RZn ferromagnets, Θ_p and T_c are found to be very close if not exactly equal.[9] The difference for TmZn is the biggest one observed in the series.

In the ordered range we have measured the magnetization when the field was applied along the three principal axes $\langle 100\rangle, \langle 110\rangle, \langle 111\rangle$; $\langle 100\rangle$ is always the easy axis and $\langle 111\rangle$ the hard one. In Fig. 2, we show the three curves obtained at $T = 1.3$ K. The moment is strongly reduced by the CEF effects, compared with the free-ion value of $7\mu_B$. This reduction is anisotropic and is due to the fact that in cubic symmetry the crystal-field Hamiltonian has important nondiagonal ma-

TABLE I. Physical constants for TmZn.

Lattice parameter at 300 K	$a = 3.516$ Å
Density at 300 K	$\rho = 8.95$ g/cm^3
Elastic constants at 300 K (in 10^{11} erg/cm^3)	$c_{11} = 9.96$ $c_{12} = 5.17_5$ $c_{44} = 5.21_5$
Elastic Debye temperature	$\Theta_e = 215$ K
Curie temperature	$T_c = 10$ K
Paramagnetic Curie temperature	$\Theta_p = 0$ K
Paramagnetic moment (free ion value $7.57\mu_B$)	$\mu_p = 7.67\mu_B$
CEF parameters	$A_4\langle r^4\rangle = -170 \pm 20$ K $A_6\langle r^6\rangle = -10 \pm 3$ K
Magnetoelastic coupling constant	$g_2^2 = 8.9 \pm 0.5$ mK
Two-ions coupling constant	$g' = -9.6 \pm 0.8$ mK

trix elements. Besides, the field dependence of the moment is very strong even along the easy fourfold axis; the spontaneous magnetization is weak and difficult to define exactly; it is about $3\mu_B$ in null internal field and increases to $6\mu_B$ at 125 kOe. Thus, studying the anisotropy of the ground-state wave function as a function of field allows us to determine the level scheme.

Another important feature of the magnetization curves is the fact that they remain equal along each direction at different low temperatures ($T<T_c$). For instance, the three curves at 4.2 K can be superimposed to the three ones shown in Fig. 2. This occurs in other RZn ferromagnets and is associated with the existence of a spin-wave energy gap Δ; in presence of CEF effects, the spontaneous moment was found to follow an $e^{-\Delta/T}$ $T^{3/2}$ law, where Δ may be obtained from the level scheme.[1,9] In TmZn, the equality of the magnetization curves for $T=1.3$, 2, 3, and 4.2 K proves that the moments are frozen in this temperature range.

B. Magnetic properties: CEF determination

We attempt, in the following, to calculate the field dependence of the magnetization in terms of molecular-field theory and cubic crystalline field. The basic Hamiltonian is taken as

$$\mathcal{H}=W\left(x\frac{O_4}{F_4}+(1-|x|)\frac{O_6}{F_6}\right)-g\mu_B J_z(H_{ex}+H_i), \tag{1}$$

where O_4 and O_6 are Stevens's operator equivalents, the expressions of which are different along the various crystallographic axes,[13] W is the scaling factor of the crystalline field, and x is a measure of the ratio of fourth- and sixth-order terms. H_i is the internal field, the exchange field being taken as $H_{ex}=n\langle M_z\rangle_T=ng\mu_B\langle J_z\rangle_T$ with the molecular-field coefficient $n=\Theta/C$. We neglect here possible biquadratic terms in the analysis of the magnetic properties. Our self-consistent calculation starts with the diagonalization of the whole Hamiltonian for any direction of the moment in the plane defined by the easy axis and the field direction, taking into account also the $J_\perp$ component. We then calculate from the level scheme, the partition function Z and the magnetization $\langle M_z\rangle$ as different thermodynamic functions of temperature using a Maxwell-Boltzmann statistics. The best agreement between the experimental and calculated low-temperature magnetization curves along the three directions determines the couple (W, x) characteristic of the scheme, the uncertainties in which are evaluated by a least-squares-fitting procedure.

In the TmZn case, the best agreement is obtained for $W=2.2$ K, and $x=-0.80$ as shown in Fig. 2. Note, at low field, the small difference due to the crystal defects. The calculations prove that in a field of about 125 kOe the moment has rotated to the field direction, and so there is a large anisotropy of the moment. This an-

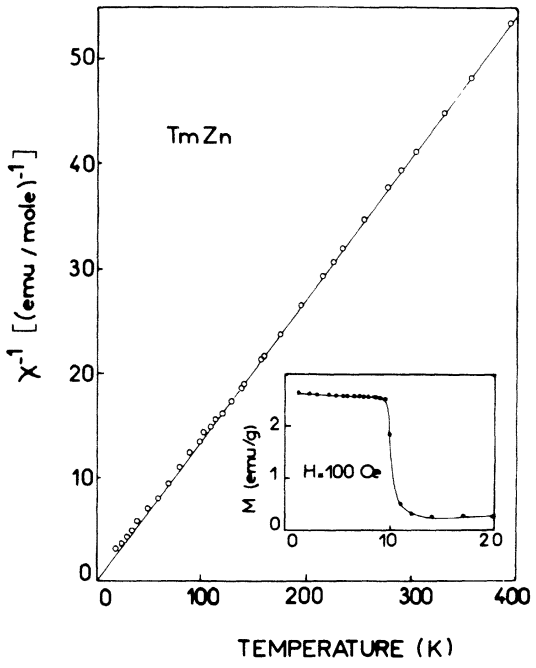

FIG. 1. Reciprocal susceptibility for TmZn. Open circles are experimental points, the line is the result of our CEF calculation. In the inset we show the determination of the Curie temperature in a low field of 100 Oe.

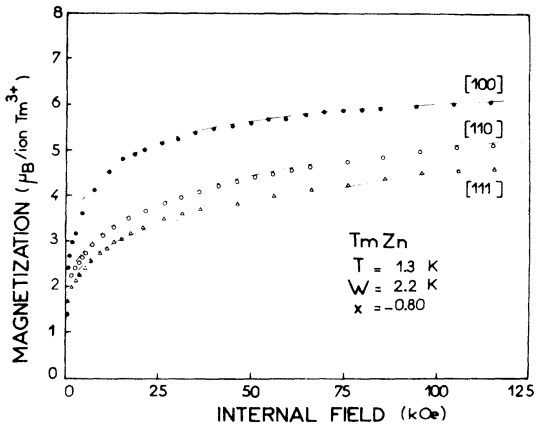

FIG. 2. Magnetization curves in internal field at 1.3 K (● : [001]; ○ : [110]; △ : [111]). The full line represents the fit along each direction with $W=2.2$ K and $x=-0.80$.

isotropy is field dependent because Eq. (1) leads to different energy levels for different axes in the presence of a magnetic field.

The couple $W = 2.2$ K and $x = -0.8$ leads to CEF parameter signs in agreement with those obtained for the RZn series. Inside the rectangular area defined in the (W, x) plane by $W = 2.2 \pm 0.2$ K and $x = -0.80 \pm 0.05$, any point gives a fit that is good along one or two crystallographic axes and only slightly imperfect along the other directions; the fit remains reasonable despite the biquadratic term neglected in Eq. (1). This may be justified by the fact that its effect is stronger on the energy's anisotropy than on the moment's values which are the only ones considered here. (A rough proof of this assumption may be obtained by use of the Callen and Callen law.[14]) In addition, we have not taken into account the forced magnetostriction, which may increase the moment and thus modify a little the scaling factor W. In the inset of the Fig. 3, we have given the level scheme corresponding to $W = 2.0$ K and $x = -0.80$.

From such a level spacing, one can calculate the thermal variation of the reciprocal susceptibility; the agreement with the experimental one is excellent (Fig. 1). In particular, the calculation confirms that there does not exist any curvature of χ^{-1} above 10 K due to Van Vleck coupling between CEF levels.

According to our analysis, the CEF ground state is a doublet Γ_3 (see insert of Fig. 3), followed by a triplet Γ_5 at 27.5 K. This level scheme is close to the one proposed for TmCd.[11] Since a Γ_3 level has no magnetic moment, TmZn has to be considered an induced moment system. Note that TmCd shows no magnetic order down to 40 mK, whereas TmZn has a $T_c = 10$ K.

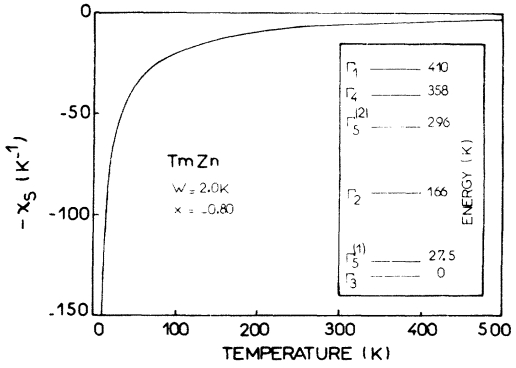

FIG. 3. Thermal dependence of the χ_s function calculated for the paramagnetic level scheme defined by $W = 2.0$ K and $x = -0.8$.

C. Lattice properties: Theory

The elastic constants as strain susceptibilities probe various quadrupole matrix elements. The measurement of their temperature dependence allows the determination of magnetoelastic coupling constants which are related to the quadrupole interaction. In the case where the CEF ground state has a non-Kramers degeneracy, we expect the corresponding symmetry elastic constant to soften; for TmZn with a Γ_3 ground state, we expect the c_{11}-c_{12} mode to soften. Such effects were observed before in TmCd.[11]

The corresponding magnetoelastic Hamiltonian is given by[11,15-18]:

$$\mathcal{H}_{me} = -g_2\left(\frac{c_{11}^0 - c_{12}^0}{N}\right)^{1/2} \sum_i \epsilon_3 O_{2i}^0 - g' \sum \langle O_2^0 \rangle O_{2i}^0 . \tag{2}$$

Equation (2) has been written for the c_{11}-c_{12} mode, $O_2^0 = 3J_z^2 - J(J+1)$ denotes the quadrupole operator, and $\epsilon_3 = (1/\sqrt{6})(2\epsilon_{zz} - \epsilon_{xx} - \epsilon_{yy})$; the other symmetry functions ϵ_2, O_2^2 can be neglected in the paramagnetic region. g_2 is the magnetoelastic coupling constant. We have included in (2) a term with a coupling constant g', which originates from quadrupole coupling other than strain-ion coupling. $\mathcal{H}_{me}$ or similar expressions for other symmetry modes have been successfully used in the past for explaining a great number of CEF effects on elastic constants, mainly near cooperative Jahn-Teller transitions.[18]

$\mathcal{H}_{me}$ in (2) gives the following temperatue dependence of the symmetry elastic constant[11,15-18]:

$$\frac{c_{11} - c_{12}}{c_{11}^0 - c_{12}^0} = \frac{1 - (g_2^2 + g')\chi_s}{1 - g'\chi_s} . \tag{3}$$

Here χ_s is the single-ion strain susceptibility. Note that $\chi_s = -f_2$, the function used in Ref. 15. $c_{11}^0 - c_{12}^0$ is the background elastic constant.

According to Eq. (3) we expect a structural (cubic-tetragonal) instability for $c_{11} - c_{12} = 0$ or for $(g_2^2 + g')\chi_s = 1$. The strain susceptibility χ_s calculated for the CEF level scheme deduced from the magnetic measurements ($W = 2.0$ K, $x = -0.80$) is plotted in Fig. 3. One notes a divergence of χ_s at low temperatures due to the degenerate Γ_3 ground state.

D. Lattice properties: Elastic-constant results

In Figs. 4–6 we show experimental results for the temperature dependence of the elastic constants. First we report, in Fig. 4, the thermal variation of $c_{11} - c_{12}$. It exhibits a very strong softening, which reaches at 13 K, 40% of the

room temperature value. A strong ultrasonic attenuation accompanies the velocity change below 30 K. We had to cut the sample from 6 mm down to 1.5 mm in order to observe echoes in the vicinity of T_c, but they completely vanished near 13 K.

In order to fit Eq. (3) to the experimental results of Fig. 4 and to extract the coupling constants g_2^2 and g', we have first to choose a suitable background. This we did from experimental results for[19] YZn: we have deduced the temperature dependence of the $(c_{11}-c_{12})_0$ curve (Fig. 4) by means of a simple affinity taking into account the mass differerence between the two compounds YZn and TmZn. Since the total level spacing for the $J=6$ manifold is more than 400 K (see the insert of Fig. 3), one still has a noticeable effect at 300 K. The final fit of Eq. (3) to our experimental results then consists of a two-parameter fit for g_2^2, g'. We obtain the following values:

$$g_2^2 = 8.9 \text{ mK}; \quad g' = -9.6 \text{ mK}.$$

With these values one attains an almost perfect fit to the experimental results as shown in Fig. 4, with a calculated curve meeting the background slightly above 400 K. Only close to T_c we note a slight deviation which might be caused by higher-order magnetoelastic terms becoming noticeable or by short-range-order effects. g' enters Eq. (3) both in the numerator and denominator; therefore, the g' value is less accurate than g_2^2. But for various combinations of g_2^2 and g' we always got $g_2^2 < |g'|$. A least-squares-fitting procedure gave small uncertainties of about 0.1 and 0.2 mK on g_2^2 and g' for a fixed couple (W, x). But the uncertainties on W and x led to an error bar Δg less than 1 mK (Table I).

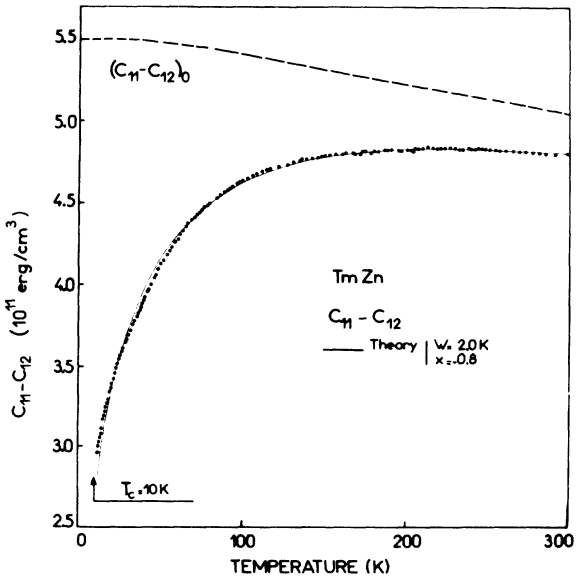

FIG. 4. Elastic constant $c_{11}-c_{12}$ as a function of temperature. Full circles are experimental points, full line is the theoretical fit. The dotted line represents the background variation of $c_{11}-c_{12}$ without CEF effect.

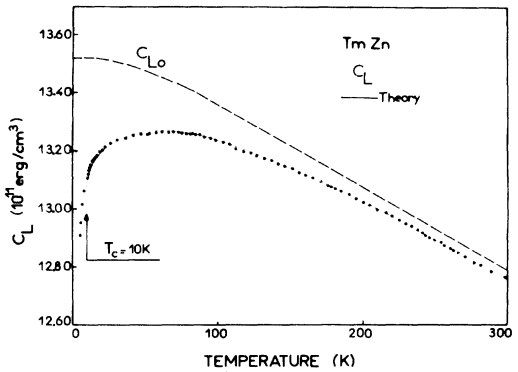

FIG. 5. Thermal dependence of the elastic constant c_L. Full circles are experimental points and the full line the theoretical fit. The dotted line represents the background variation.

In Fig. 5, we show analogous results for $c_L = \frac{1}{2}(c_{11}+c_{12}+2c_{44})$, the longitudinal mode in a $\langle 110 \rangle$ direction. One notes a much smaller softening

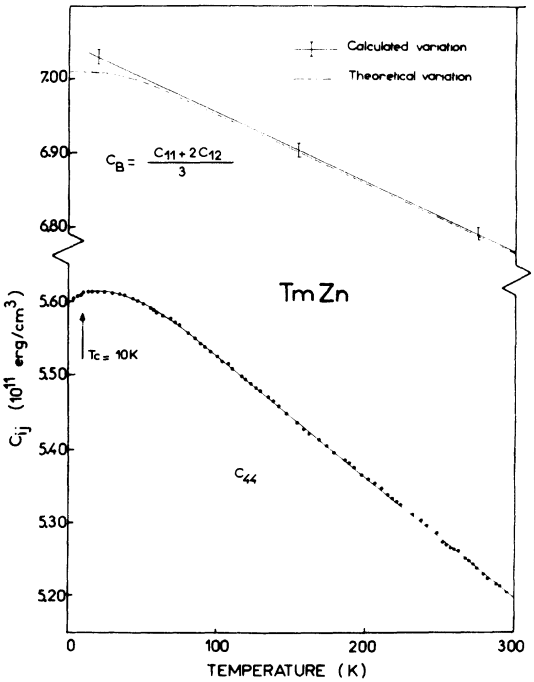

FIG. 6. Thermal variation of the elastic constant c_{44} and of the bulk modulus c_B. The full line follows the temperature variation of the c_{44} mode in YZn. The calculated dependence of c_B from our experiments (full line) deviates only slightly below 40 K from the corresponding variation for YZn (broken line).

in this case of about 1.3% at 10 K. Below T_c the echoes were more damped and this influence of domain-wall stress effects on the elastic constants is clearly visible. We made an analogous fit for c_L as for $c_{11}-c_{12}$. The background c_L^0 was again estimated from the corresponding results for YZn.[19] With $c_L = c_B + \frac{1}{6}(c_{11}-c_{12}) + c_{44}$ and $c_B = \frac{1}{3}(c_{11}+2c_{12})$, c_{44} showing no softening, we again get an excellent fit to our experimental results, using the same values for g_2^2 and g' as above. This demonstrates the consistency of our analysis (energy level scheme and coupling constants).

Figure 6 shows experimental results for the shear mode c_{44} and the bulk modulus c_B. For the c_{44} mode we practically observe no CEF effects, indicating that the corresponding magnetoelastic coupling constant g_3 is quite small.[15] Therefore, we shall not discuss this mode any further here, except to remark that below T_c one observes again domain-wall stress effects. From the three experimentally determined $c_{11}-c_{12}$, c_{44}, and c_L, we have calculated the temperature dependence of the bulk modulus c_B. This is shown as the full line in Fig. 6. We compare this to c_B from YZn,[19] which corresponds to the dotted line and which was matched to the full line at 300 K. The agreement is good except at low temperatures, where the large change in $c_{11}-c_{12}$ can induce large errors. Note that in linear magnetoelastic theory, which was used in Eq. (2), the strain susceptibility for c_B is zero as discussed before.[15]

IV. CONCLUSIONS

The successful analysis reported in Sec. IIID produced a number of important physical parameters. From these, we can draw a number of important conclusions, which we would like to discuss now.

A. CEF parameters A_4 and A_6

As for other RZn compounds,[20] W and x lead to corresponding parameters $A_4\langle r^4\rangle$ and $A_6\langle r^6\rangle$, both negative:

$$A_4\langle r^4\rangle = -170 \pm 20 \text{ K}$$

$$A_6\langle r^6\rangle = -10 \pm 3 \text{ K}.$$

These values are very different from the results of a point-charge estimate which leads to a small positive fourth-order term and a negligible sixth-order one, even taking into account the density of conduction electrons in the ligands obtained by augmented-plane-wave (APW) calculations.[10] With several authors[6,21] we find that the field on the $4f$ shell is due mainly to the conduction electrons of $5d$ character (e_g type) in the $4f$ ion itself. This opposite-sign contribution to the anisotropic exchange is found to be larger than the Coulomb contribution to $A_4\langle r^4\rangle$ in the RZn series.[9] As in the case of PrZn and NdZn,[20] its magnitude is stronger than in RZn compounds with rare earths in the middle of the series. This variation in the $4f$ electron number may be due to the orthogonal wave functions of the band and the $4f$ shell. The sixth-order term cannot presently be interpreted, its large magnitude is of the same order as in[4] ErZn and may be related to anisotropic exchange effects.

Note that the strong nondiagonal matrix elements in the cubic CEF Hamiltonian lead to an important reduction of the moment. On the other hand, in the RZn compounds as in isomorphous ones the strong CEF parameters induce a level spacing larger than the ordering temperature. Thus, according to the level scheme, the anisotropies of the magnetization and of the energy are strongly field dependent.

B. Magnetoelastic coupling constant g_2^2

In the case of the rare-earth antimonides, the magnetoelastic coupling constant g_2 followed rather closely an effective point charge model description[15] in a similar way as the CEF parameters A_4, A_6. This is not the case here, where we get $g_2^2 = 57$ mK using a ligand charge of $Z \simeq 1$[22] which is far off from the experimentally determined value of 8.9 mK, as quoted above. A similar observation can be made for TmCd.[11] Note that from the elastic constants one can only determine the square of the coupling constant g_2. A measurement of the actual lattice distortion can however determine the sign of g_2. From the quoted value of g_2^2 we can easily estimate the expected c/a ratio for $T=0$. With

$$E = \tfrac{1}{2}c_0\epsilon_3^2 - g_2(c_0N)^{1/2}\epsilon_3\langle \Gamma_3^1|\, O_2^0|\, \Gamma_3^1\rangle, \tag{4}$$

one obtains through minimalization of the energy

$$\epsilon_3 = g_2(N/c_0)^{1/2}\langle \Gamma_3^1|\, O_2^0|\, \Gamma_3^1\rangle.$$

With the matrix element $\langle \Gamma_3^1|\, O_2^0|\, \Gamma_3^1\rangle = 36$, we get $|c/a - 1| = 0.6\times10^{-2}$. This estimate could be changed by inclusion of higher-order terms. An effect of this magnitude can easily be observed with x rays. Another method to determine magnitude and sign of the magnetoelastic coupling constant g_2 is by magnetostriction experiments in the paramagnetic phase as demonstrated for[23] TmCd; $c/a - 1 = -0.7\times10^{-3}$ in agreement with its absolute value[11] and corresponding to a contraction along the c axis. Such experiments are underway on TmZn.

C. Effective quadrupole-quadrupole interaction

Equations (2) and (3) show that elastic constants determine an effective $q=0$ quadrupole interaction constant $G(q=0)=g_2^2+g'$. For TmCd, $G=1.68$ mK (Ref. 11) and for TmZ, $G=-0.7$ mK. Using Eq. (3) this leads in the case of TmCd to a transition temperature $T_a=2.3$ K, not far from the observed structural transition $T_a=3.16$ K. In the case of TmZn, there is no structural transition, but c/c_0 attains the limiting value $(g_2^2+g')/g'=0.073$. It is the near cancellation of g_2^2 and g' which prevents a structural transition for TmZn in absence of exchange interactions. It is of interest to speculate on the physical nature of the quadrupole interaction described by the g' coupling constant. For CsCl as well as NaCl structures, the $q=0$ optical-phonon branch cannot couple.[17] Apart from self-energy contributions which for a Debye solid amount to $-\frac{1}{3}g_2^2$,[18] there must be other mechanisms operative both for TmCd and TmZn. One obvious possibility for good conductors such as TmCd and TmZn is the aspherical Coulomb scattering. There is a rapidly growing literature giving experimental and theoretical evidence for this type of mechanism.[18,24] The accumulation of APW calculations on nonmagnetic compounds with CsCl structure proves the main importance of the e_g band, always close to the Fermi level[10,25]; its exact position determines the CsCl phase stability or the existence of a martensitic transformation.[26] In RZn compounds, at the ordering temperature, a f-d quadrupolar coupling may split the e_g band degeneracy and explain the spontaneous magnetostriction.[9] In RCd the martensitic transformation of LaCd proves that the CsCl phase stability is weaker than in RZn; this may explain the existence of the transition which occurs in TmCd according to the CEF level scheme without magnetic ordering.

We go on with the study of the elastic constants in the RZn series. A preliminary result is the agreement on the order of magnitude of the tetragonal distortion between elastic-constant and low-temperature x-ray experiments,[27] in particular for DyZn and ErZn.

---

*Supported in part by NSF.

[1]K. Kanematsu, G. T. Alfieri, and E. Banks, J. Phys. Soc. Jpn. 26, 244 (1969); P. Morin and J. Pierre, Solid State Commun. 13, 537 (1973); Phys. Status Solidi A 17, 479 (1973); R. Aleonard, P. Morin, and J. Pierre, Coll. Intern. du C.N.R.S. "Physics in High Magnetic Fields," Grenoble, 1974 (unpublished).

[2]P. Morin and J. Pierre, Phys. Status Solidi A 21, 161 (1974).

[3]P. Morin and A. De Combarieu, Solid State Commun. 17, 975 (1975); P. Morin, J. Pierre, and J. Chaussy, Phys. Status Solidi A 24, 425 (1974).

[4]P. Morin, J. Pierre, J. Rossat-Mignod, K. Knorr, and W. Drexel, Phys. Rev. B 9, 4932 (1974).

[5]G. Williams and L. Hirst, Phys. Rev. 185, 407 (1969).

[6]H. C. Chow, Phys. Rev. B 7, 3404 (1973).

[7]J. Høg and P. Touborg, Phys. Rev. B 9, 2920 (1974); Phys. Rev. Lett. 33, 775 (1974).

[8]R. J. Birgeneau, E. Bucher, J. P. Maita, L. Passell, and K. C. Turberfield, Phys. Rev. B 8, 5347 (1973).

[9]P. Morin, thesis (University of Grenoble, AO C.N.R.S. 9323, 1975) (unpublished).

[10]M. Belakhovsky, J. Pierre, and D. K. Ray, Phys. Rev. B 6, 939 (1972).

[11]B. Lüthi, M. E. Mullen, K. Andres, E. Bucher, and J. P. Maita, Phys. Rev. B 8, 2639 (1973).

[12]H. J. Skimin, J. Acoust. Soc. Am. 32, 12 (1961); E. P. Papadakis, *ibid.* 42, 1045 (1967).

[13]K. R. Lea, M. J. M. Leask, and W. P. Wolf, J. Phys. Chem. Solids 23, 1381 (1962).

[14]H. B. Callen and E. Callen, J. Phys. Chem. Solids 27, 1271 (1966).

[15]M. E. Mullen, B. Lüthi, P. S. Wang, E. Bucher, L. D. Longinotti, J. P. Maita, and H. R. Ott, Phys. Rev. B 10, 186 (1974).

[16]M. Kataoka and J. Kanamori, J. Phys. Soc. Jpn. 32, 113 (1972).

[17]P. Levy, J. Phys. C 6, 3545 (1973).

[18]G. A. Gehring and K. A. Gehring, Rept. Prog. Phys. 38, 1 (1975).

[19]R. J. Schiltz, Jr., T. S. Prevender, and J. F. Smith, J. Appl. Phys. 42, 4680 (1971).

[20]P. Morin and J. Pierre, Phys. Status Solidi A 30, 549 (1975).

[21]K. C. Das and D. K. Ray, Solid State Commun. 8, 2025 (1970).

[22]For this estimate we took the point-charge model expression $g_2=4\sqrt{2}(Ze^2/d^3)\langle r^2\rangle\alpha_J(N/c_0)^{1/2}$; $(d=\frac{1}{2}\sqrt{3}\,a)$.

[23]H. R. Ott and K. Andres, Solid State Commun. 15, 1341 (1974); H. R. Ott and B. Lüthi, AIP Conf. Proc. (to be published).

[24]A. Fert and A. Friederich, AIP Conf. Proc. 20, 466 (1974).

[25]A. Hasegawa and J. Kubler, Z. Phys. 269, 31 (1974); A. Hasegawa, B. Bremicker, and J. Kübler, Z. Phys. B 22, 231 (1975).

[26]H. Ihring D. T. Vigren, J. Kubler, and S. Methfessel, Phys. Rev. B 8, 4525 (1973).

[27]P. Morin and J. Pierre, Phys. Status Solidi A 21, 161 (1974); J. Laforest, P. Morin, J. Pierre, and J. S. Shah, C. R. Acad. Sci. (Paris) B 277, 353 (1973).